DYSTONIA

TYPE Original Research
PUBLISHED 13 November 2025
DOI 10.3389/dyst.2025.15390

OPEN ACCESS

EDITED BY
Roy Sillitoe,
Baylor College of Medicine,
United States

*CORRESPONDENCE
Terence D. Sanger,
terry@sangerlab.net

†These authors have contributed equally to this work

RECEIVED 06 August 2025
REVISED 24 October 2025
ACCEPTED 31 October 2025
PUBLISHED 13 November 2025

CITATION
Seyyed Mousavi SA, Javadzadeh S, Asadi M, Ivry RB and Sanger TD (2025) Behaviorally coupled oscillations reveal distinct timing roles of basal ganglia and cerebellothalamic circuits in dystonia. *Dystonia* 4:15390.
doi: 10.3389/dyst.2025.15390

Behaviorally coupled oscillations reveal distinct timing roles of basal ganglia and cerebellothalamic circuits in dystonia

S. Alireza Seyyed Mousavi[1], Sina Javadzadeh[2†], Mehrnaz Asadi[1†], Richard B. Ivry[3] and Terence D. Sanger[1,4*]

[1]Department of Electrical Engineering and Computer Science, University of California, Irvine, Irvine, CA, United States, [2]Department of Biomedical Engineering, University of California, Irvine, Irvine, CA, United States, [3]Department of Psychology, University of California, Berkeley, Berkeley, CA, United States, [4]Department of Neurology, Children's Hospital Orange County, Orange, CA, United States

As part of a deep brain stimulation (DBS) procedure, direct electrophysiological recordings from thalamic and basal ganglia circuits were obtained from a pediatric participant with secondary dystonia to examine the neural mechanisms of motor timing. The participant performed a two-phase repetitive timing task that began with synchronization to a series of externally presented auditory cues, followed by a continuation phase in which the participant maintained the movement rhythm without external guidance. Simultaneous recordings from stereoelectroencephalography (sEEG) leads implanted in the globus pallidus internus (GPi), subthalamic nucleus (STN), ventral oralis (Vo), centromedian nucleus (CM), and thalamic nuclei receiving projections from the cerebellum (ventral intermediate nucleus (VIM) and centrolateral nucleus (CL)) revealed behaviorally relevant neural dynamics. Local field potentials (LFPs) from recorded nuclei exhibited strong, time-locked responses during the synchronization phase, with reduced amplitudes during the continuation phase. Time-frequency analysis showed consistent power increases around the corresponding mean of the inter-response intervals (IRIs) in both behavioral output and neural signals, suggesting frequency-specific entrainment across circuits. These findings suggest of cerebellar-thalamic and basal ganglia contributions to temporal coordination.

KEYWORDS

deep brain stimulation, dystonia, cerebellar dysfunction, local field potentials, cerebellum and basal ganglia

Introduction

Cerebellar dysfunction is associated with deficits in motor timing and sensorimotor integration, leading to movement disorders characterized by temporal instability and impaired predictive control [1, 2]. Patients with cerebellar lesions exhibit ataxia, a loss of coordination. One feature of this disorder is elevated temporal variability in patterns of muscular activation and in the timing of rhythmic movements [3, 4]. These findings, coupled with other evidence implicating the cerebellum in temporal processing [5, 6], suggest that cerebellar circuits play a key role in encoding movement timing which can help stabilize rhythmic behaviors.

Dystonia is a neurological condition characterized by persistent muscle contractions that result in involuntary twisting motions and abnormal body postures [7]. While dystonia has historically been attributed to basal ganglia dysfunction, certain cases of dystonia have been shown to involve cerebellar pathology [8–12], and experimental studies have demonstrated that cerebellar lesions or cerebellectomy can abolish dystonic symptoms in animal models [13]. To date, direct electrophysiological recordings with high temporal resolution from human basal ganglia, cerebellum, or structures receiving direct input from the cerebellum remain limited. Prior studies have focused on non-invasive methods such as fMRI-based connectivity analyses, and thus lack the temporal resolution necessary to capture oscillatory dynamics within these regions [14, 15].

In this study, we tested a participant with dystonia on a repetitive timing task. From stereoelectroencephalography (sEEG) leads, we examined local field potentials (LFPs) recorded in the basal ganglia and thalamic structures, including thalamic regions receiving cerebellar projections (ventral intermediate nucleus (VIM) [16–20] and centrolateral nucleus (CL) [21–23]). Of particular interest is the VIM. This thalamic nucleus receives excitatory input from the dentate nucleus (DN) and has been shown to encode information for precise event timing and rhythm coordination [16].

Materials and methods

Participant and experimental setup

A male participant (age 14) diagnosed with generalized dystonia, who underwent staged implantation of DBS leads as part of his clinical treatment [24, 25], participated in this study. Prior to the lead implantation surgery, written informed consent was obtained from his legal guardians, in compliance with HIPAA regulations. This consent authorized the use of his electrophysiological data for research purposes. The study protocols were approved by the institutional review boards at Children's Hospital of Orange County; Rady Children's Health.

The participant performed 24 trials of a repetitive timing task. Each trial lasted 18 s and was divided into two distinct phases. In the first 6 s (synchronization phase or S-phase), an auditory metronome provided periodic tones every 600 ms (i.e., 1.667 Hz), and the participant was prompted to synchronize joystick movements with the tones. The metronome was then turned off and the participant continued the movement, attempting to maintain the same rhythm established during the synchronization phase for an additional 12 s (continuation phase or C-phase), relying solely on internal timing mechanisms. The joystick position and auditory metronome were sampled at approximately 3 kHz throughout the trial.

Prior to the first trial, the experimental setup was introduced to the participant and he was instructed that the objective is to synchronize his joystick manipulation with the auditory tone during the S-phase and then keep the same rhythm during the C-phase until the end of the trial (Figure 1).

Electrophysiological recordings

A total of 10 temporary sEEG depth leads (AdTech MM16C; AdTech Medical Instrument Corp., Oak Creek, WI, United States), approved by the FDA for clinical use, were implanted bilaterally into potential DBS targets consisting of globus pallidus internus (GPi), subthalamic nucleus (STN), ventral oralis (Vo), centromedian nucleus (CM), CL, and VIM using standard stereotactic procedure [24, 25]. Figure 2 demonstrates targeted brain nuclei and sEEG electrodes used for implantation.

Each lead features six low-impedance (1–2 kΩ) ring macro-contacts, each 2 mm in height and spaced 5 mm apart, along with ten high-impedance (70–90 kΩ) microwire electrodes (50-μm diameter) known as micro-contacts. The micro-contacts are arranged in groups of two or three, evenly distributed around the lead's circumference and positioned midway between adjacent pairs of macro-contacts. The leads were attached to Adtech Cabrio^{TM} connectors, which include a custom unity-gain preamplifier for each micro-contact to minimize noise and motion artifacts. Micro-contact data were sampled at approximately 24 kHz using a system equipped with a PZ5M 256-channel digitizer and RZ2 processor and stored in an RS4 high-speed data storage system (Tucker-Davis Technologies Inc., Alachua, FL, United States).

Data preprocessing

LFPs are extracted through a three-stage preprocessing pipeline. First, a 0.05 Hz high-pass filter removes DC component. Second, common-mode noise is eliminated by subtracting the median of the 10 micro recordings, scaled to each channel independently. Finally, a 4th-order Butterworth low-pass filter (30 Hz) extracts LFP signals.

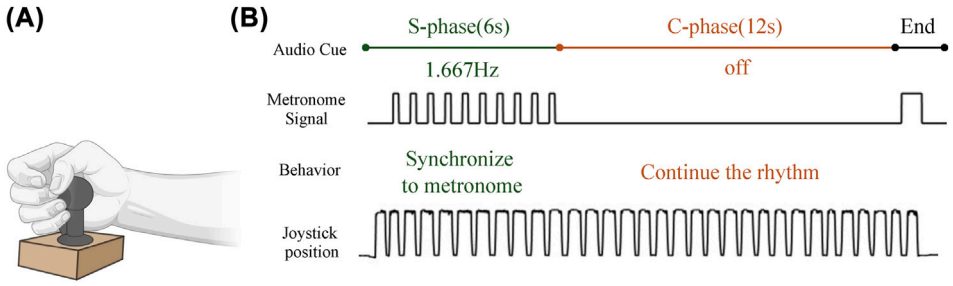

FIGURE 1
Task protocol. **(A)** Experimental setup. Created in BioRender. Seyyedmousavi, S. (2025). **(B)** Task protocol consisting of two phases: the "S-phase," where a metronome is played at 1.667 Hz and the participant synchronizes his movements with it, and the "C-phase," where the participant maintains the same rhythm without the metronome until the end tone is heard.

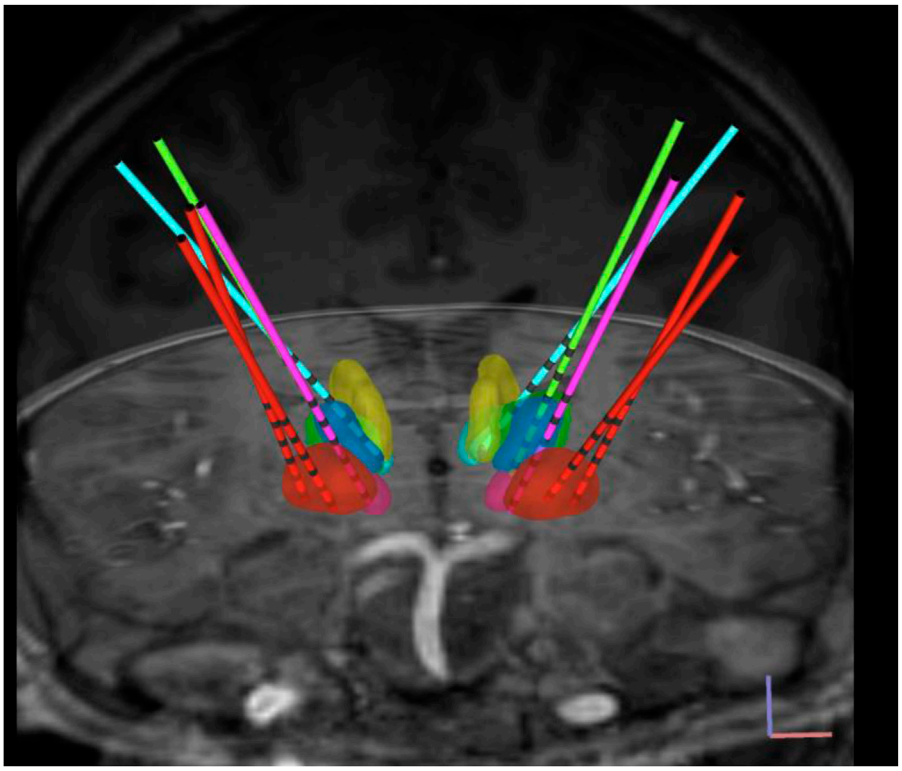

FIGURE 2
Targeted brain nuclei and sEEG electrodes. View of sEEG electrodes in bilateral brain nuclei: GPi (red), Vo (blue), STN (pink), VIM (green), CM (yellow), and CL (cyan); normalized scans visualized onto the Montreal Neurological Institute (MNI) space. Deep brain region boundaries were defined with the DISTAL atlas.

Statistical analysis

All analyses were performed in MATLAB. For behavior, we computed, per trial and phase, the mean IRI and IRI standard deviation and compared phases using the Wilcoxon signed-rank test. Statistical significance was set at $p < 0.05$. For neural data, movement-aligned LFPs were baseline-normalized per channel and summarized by peak-to-peak amplitude within a predefined window around movement onset. Channels were averaged within region, yielding one peak-to-peak value per trial, phase, and region. We compared S-phase vs C-phase with the Wilcoxon signed-rank test per region and controlled multiple comparisons

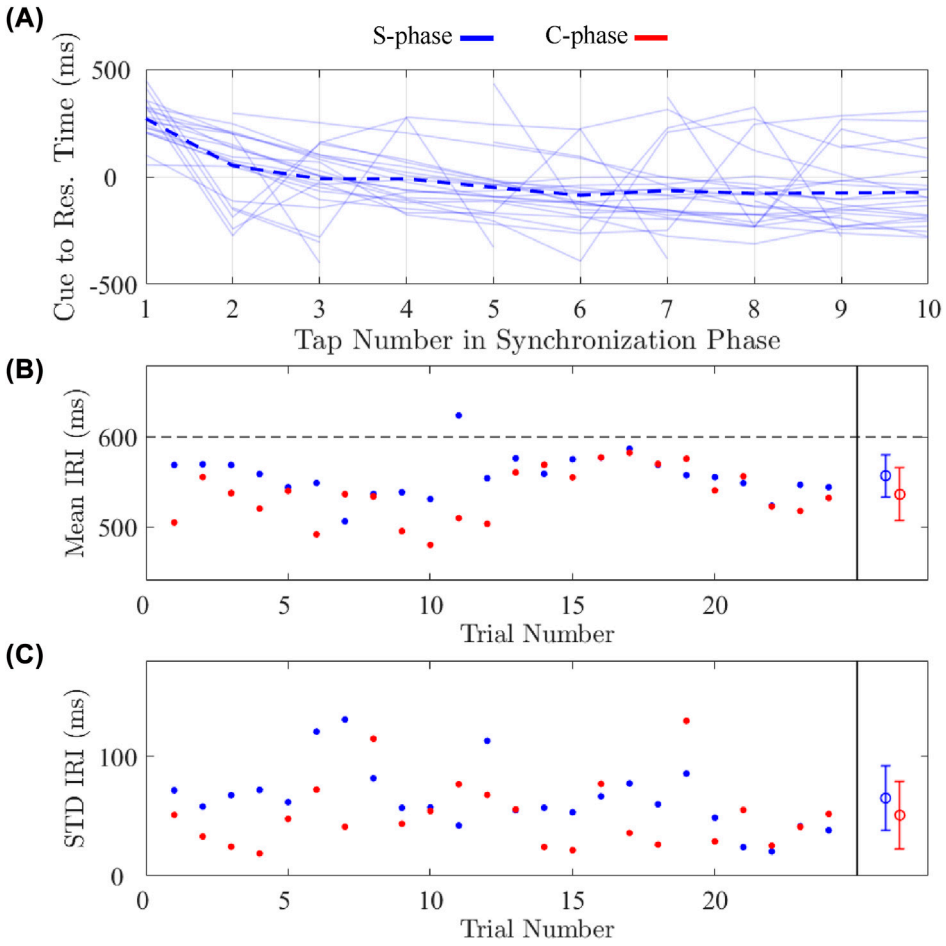

FIGURE 3
Behavioral results. **(A)** Time difference between the auditory cue and each joystick movement during the S-phase. Individual trial traces are shown in light solid blue, with the across-trial mean overlaid in dark dashed blue. An initial lag during the first few movements which then converge to a lead in the later responses, reflecting rapid stabilization in response to the audio cue. **(B)** Mean IRI per trial in both S-phase and C-phase (circles), with the overall mean (and SD of the mean) displayed after the black divider. Mean IRIs remain close to, but slightly deviate from, the 0.6-s auditory interval. **(C)** Standard deviation of the IRIs per trial.

using Benjamini–Hochberg FDR across regions ($q < 0.05$). Regions exhibiting significant within-trial differences after FDR correction were interpreted as showing robust phase-dependent modulation of LFP amplitude.

Results

Participant performance and motor consistency during repetitive timing task

The participant was able to perform the repetitive timing task. As can be seen from the joystick position data depicted in Figure 1, the participant tended to make discrete out and back movements, with a pause at the center position prior to each movement. Figure 3A illustrates the time difference between the auditory cue and each corresponding joystick manipulation during the S-phase. The average time difference is positive during the first three intervals, indicating that, with the onset of the metronome, the movements initially lagged behind the tones. However, in subsequent intervals, the time difference becomes negative and stabilizes, suggesting that the responses began to consistently lead the auditory cue.

Figures 3B,C present the mean and standard deviation of the inter-response intervals (IRIs) for each trial. The participant moved significantly faster during the C-phase compared to the S-phase (Wilcoxon signed-rank, $p < 0.001$). In both phases, the movement rate was also faster than the specified interval, with mean IRIs of 557 ms in the S-phase and 536 ms in the C-phase. This behavior suggests that, while the metronome provided a rough guide to the desired rate, the participant relied more on an endogenous signal to establish the temporal pattern

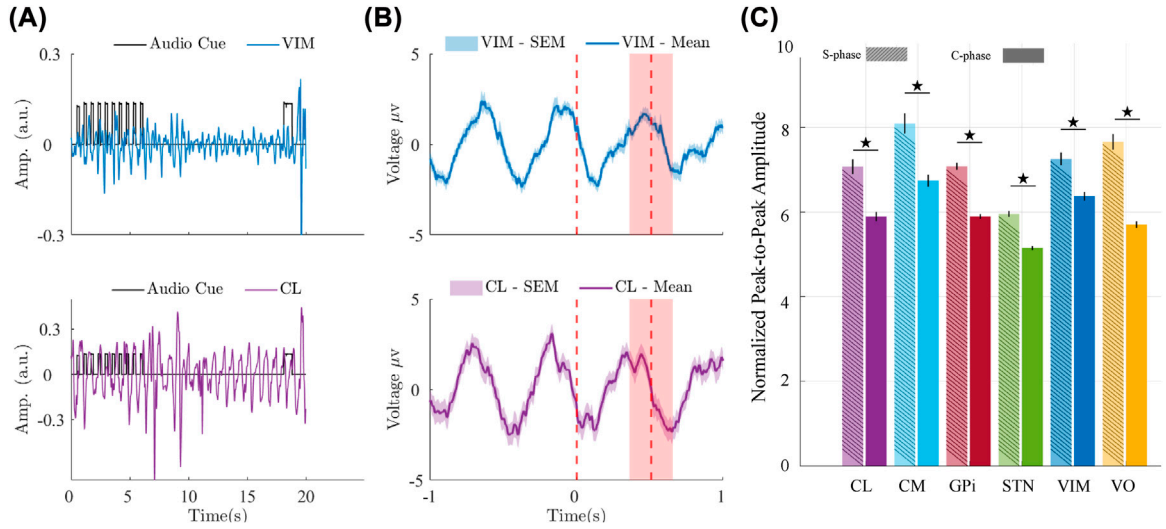

FIGURE 4
LFP responses across thalamic and basal ganglia regions during repetitive timing task. **(A)** Example LFP traces from the VIM and CL, plotted alongside the auditory metronome signal during a single trial. Rhythmic LFP activity is observed during the S-phase and continues into the C-phase with reduced amplitude. **(B)** Example of event-triggered average LFP responses in VIM (top) and CL (bottom), aligned to joystick movement onset across all trials. Red dashed lines indicate the average onset times of the next joystick movements across trials, while the red shaded region shows the corresponding standard deviation. LFP Traces span from 1 s before to 1 s after movement onset. **(C)** Peak-to-peak amplitudes of movement-aligned LFPs during the S-phase and C-phase for each recorded region. Each bar shows the average amplitude across trials for the respective phase. Black vertical lines show SEM of the peak-to-peak amplitudes across trials. Asterisks indicate regions showing significance after BH-FDR correction across regions ($q < 0.05$).

for each trial. On average, IRI variability is lower during the C-phase than the S-phase (Wilcoxon signed-rank, $p < 0.05$), likely due to the initial challenge of establishing the desired rate and synchronization of the initial movements with the metronome. This reduction in variability may also reflect increased rhythmic consistency during internally generated timing. The Weber fraction (SD/Mean × 100) was 9.45% during the C-phase. This value is higher than that typically observed in young adults on repetitive movements task (e.g., 5%), a difference that may arise from the difference in age, neurological condition, and/or response device.

Behaviorally relevant neural activity

LFP activities from all recorded regions exhibit rhythmic activity that is aligned with the response rhythms during the S-phase and persists, though at reduced amplitude, into the C-phase. Figure 4A shows example LFP recordings from the VIM and CL, along with the auditory metronome signal, during a single trial.

To assess the relationship between neural signals and movement timing across all trials, we performed event-triggered averaging of the LFPs time-locked to joystick movement onset. Figure 4B displays examples of these averages for VIM (top panel) and CL (bottom panel), aligned from 1 s before to 1 s after movement onset. Both regions, as well as other regions exhibit consistent time-locked modulations, suggesting functional coupling between the neural activity and motor output.

To compare neural response amplitude across task phases, we calculated the average peak-to-peak amplitude of movement-aligned LFPs during the S-phase and C-phase. Figure 4C summarizes these amplitudes across all recorded regions. LFP responses were significantly stronger during the S-phase than the C-phase in all regions. This could reflect neural activity to the tones, increased neural responsiveness when the movement is accompanied by an auditory stimulus, or activity monitoring the phase relationship between the tones and movement.

Oscillatory dynamics in motor behavior and LFP signals

To characterize the frequency-specific dynamics of behavior and neural signals during the task, we created time-frequency representations (scalograms) of joystick movements and LFP activity. Figure 5A demonstrates scalogram representation of joystick movement and example LFP recordings from the VIM and CL during a single trial. The joystick signal exhibited sustained power at approximately 1.8 Hz throughout both the synchronization and continuation phases, a value that is

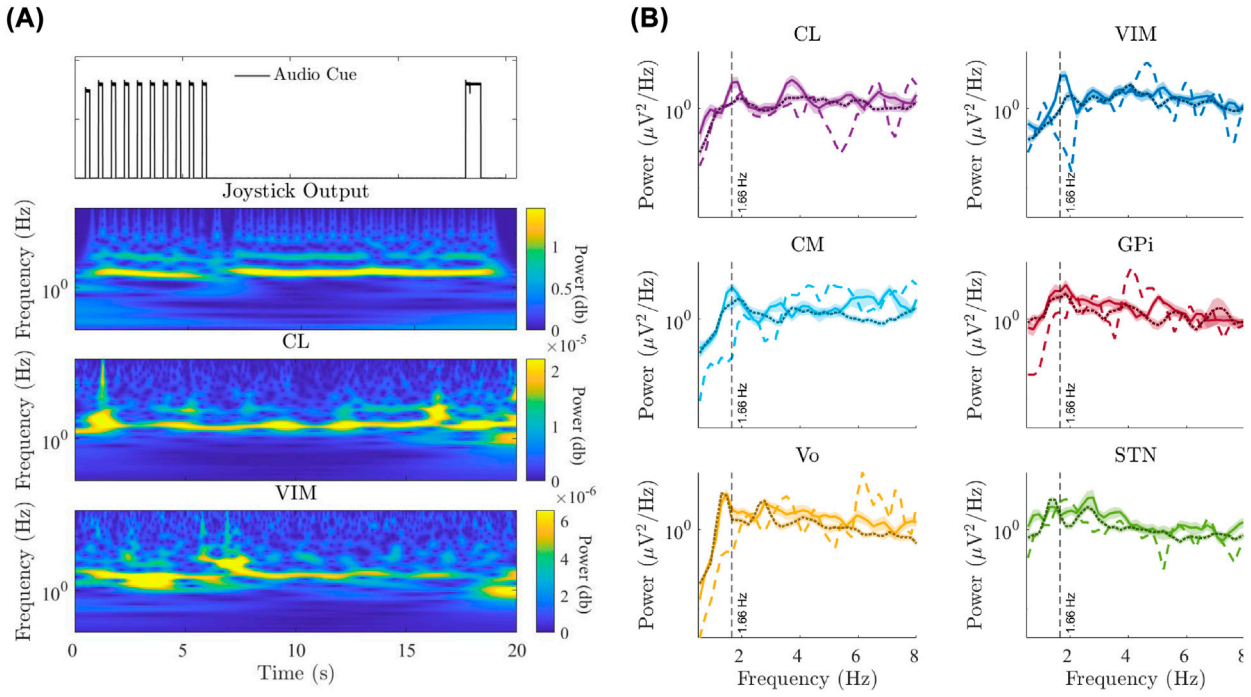

FIGURE 5
Time-frequency analysis of motor output and LFP signals. **(A)** Example time-frequency representations (scalograms) of joystick position and LFPs from the VIM and CL during a single trial. All signals show sustained power near the task frequency of approximately 1.667 Hz during both the S-phase and C-phase. **(B)** Power spectral densities (PSDs) averaged across all trials and phases (S-phase and C-phase) for each recorded region during the task, compared to baseline recordings from the same regions. Solid (S-phase), dotted (C-phase), and dashed (baseline) lines demonstrate the mean power. Shaded areas demonstrate standard error mean (SEM). Prominent peaks are observed near the task frequency during task phases.

consistent with the mean IRI. Neural recordings from both VIM and CL showed corresponding oscillatory power at approximately the same frequency, which was present in the S-phase and remained stable throughout the C-phase.

Figure 5B shows average power spectral densities (PSDs) across all trials for each recorded region during both S-phase and C-phase, overlaid with baseline PSDs from the same regions. Baseline activity was defined as 20 s resting period prior to task onset during which the participant remained still and no external cues were presented. LFP recordings from all regions demonstrated a prominent peak near the task frequency (1.667 Hz) during task performance for both S-phase and C-phase.

Discussion

Rapid transition from sensory cued to internally generated timing

The early lag observed during the initial joystick manipulations of the S-phase (Figure 3A), followed by a transition to a stable negative time difference, reflects a rapid shift from reactive to anticipatory timing. This pattern is consistent with cerebellar-mediated predictive control by which the motor system utilizes internal timing mechanisms to generate responses timed to align with the expected sensory events [1, 26]. The fact that the participant adopted a rate faster than the metronome during the S-phase and maintained this rate during the C-phase further indicates that performance was primarily based on internal timing signals rather than via entrainment. While the metronome helps establish the rate, there is likely little error correction based on the phase differences between the tones and movements given that the S-phase was relatively short.

Cerebellothalamic circuit dynamics and frequency-specific signatures of rhythmic timing

The LFP data in Figure 4 highlights the engagement of all recorded regions – with example plots from VIM and CL–during externally cued and internally generated movement. These regions (i.e., VIM and CL) receive projections from the cerebellum [17, 18, 20], and have been implicated in

cerebellar-based timing through anatomical and functional studies. Behavioral evidence also supports cerebellar contributions to subsecond interval timing and sensory-guided coordination [1, 27]. The presence of rhythmic, time-locked activity aligned to movement onset (Figure 4B) suggests that these regions are actively involved in organizing movement timing. However, whether these LFP modulations primarily reflect motor execution or internal timing processes remains unclear, as both components are temporally aligned in this task.

The consistently higher peak-to-peak amplitudes observed during the S-phase across all regions (Figure 4C) reflect enhanced neural responsiveness when the auditory metronome cue is present. This pattern could reflect a feedback process whereby the auditory feedback is used to update temporal predictions [26, 28]. Alternatively, it could reflect neural activity to the tones or increased neural responsiveness when movement is accompanied by a stimulus that specifies an exogenous goal. The persistence of oscillatory activity into the C-phase – despite the absence of metronome cues – raises the possibility that cerebellar-recipient thalamic nuclei contribute to internally sustained timing processes.

While our data do not isolate the source of internally generated timing, the maintenance of phase-locked LFP activity during the C-phase may reflect ongoing contributions from internal circuits. These may include cerebellar mechanisms operating in a predictive mode, as well as possible involvement of parallel systems such as basal ganglia-thalamic loops, which have been implicated in sustaining rhythmic behavior in the absence of sensory input [29–32]. Interestingly, Vo and VIM exhibited movement-related oscillations at slightly lower frequencies than other regions. One possible explanation, which requires further investigation, is that this pattern reflects their distinct afferent inputs and integrative roles within the motor timing network. Given that these thalamic nuclei receive temporally smoothed input from the cerebellum and basal ganglia, the slower oscillatory components may represent an integration process that supports predictive control over extended intervals.

The spectral analyses in Figure 5 reveal task-related increases in power at the behavioral frequency in both motor output and recorded LFPs. This frequency-specific response was consistently observed in most recorded regions including VIM and CL. The presence of this frequency-specific response supports the notion that the basal ganglia and cerebellum and its thalamic projections contribute to the timing of these repetitive movements.

These findings are consistent with prior studies reporting enhanced low-frequency power in cerebellar and thalamic regions during repetitive tapping and motor sequencing tasks [5, 33, 34]. The alignment between spectral peaks in neural activity and behavioral rhythm supports the idea of coordinated circuit-level mechanisms for timing, potentially involving synchronized activity across cerebellar-thalamocortical loops.

Clinical relevance for DBS targeting

We provide evidence that both basal ganglia and cerebellar projections in the thalamus are engaged during a repetitive timing task, exhibiting precisely timed neural modulations correlated with behavior. Although dystonia is clinically characterized by abnormal co-contraction rather than rhythmic movement, impaired temporal coordination within subcortical circuits may contribute to this disorganization. Thus, understanding how these networks generate and maintain temporal structure may inform how DBS modulates circuit dynamics to restore stable motor output [35].

Our results support the emerging view that cerebellothalamic circuits play a central role in motor timing and interact with basal ganglia pathways to regulate temporal precision. The presence of task-frequency-aligned activity and movement-locked modulations across these regions underscores their role in supporting temporally structured motor behavior. While these neural responses exhibit rhythmicity, this likely reflects iterative operation of an internal interval-timing mechanism rather than an autonomous oscillator. In this framework, thalamic regions receiving cerebellar input - particularly VIM and CL - may serve as key relay sites for transmitting timing-related signals within a distributed motor network. Future studies combining electrophysiology and clinical outcomes could determine whether modulating these pathways through DBS contributes to improved temporal stability and motor control in dystonia.

Limitations and future work

Despite the insight gained from these findings, the current study has several limitations. The single-participant nature of the dataset constrains generalizability. Another potential limitation is that the participant's dystonia could have influenced motor performance or neural activity. However, the influence of dystonic symptoms on task performance was minimal. The experimental paradigm required only small, controlled joystick movements, which were largely unaffected by dystonic posturing. Furthermore, since our analyses focused on low-frequency dynamics (1–2 Hz), it is unlikely that dystonia-related activity in other frequency bands contributed substantially to the observed neural responses. Importantly, dystonic activity is generally considered task-unrelated and does not exhibit correlation with task timing or movement-related oscillations. Therefore, the rhythmic patterns observed here likely reflect task-evoked neural dynamics rather than dystonia-associated background activity. Expanding this approach to multi-subject datasets will be critical to evaluate the generalizability of these findings and to determine whether deep brain stimulation

(DBS) can modulate specific timing-related neural dynamics to restore temporal precision in movement disorders.

A major challenge in interpreting time-locked neural activity during movement is the confounding of internal timing, motor execution, and feedback-related processes. As shown in Figure 5B, the spectral analyses were quite similar for all of the recorded sites. While this might indicate that repetitive movements emerge from network dynamics of cortical and subcortical regions, it is also possible that the recorded regions have differential roles in temporal control, movement execution, and feedback related processes. Future work should incorporate task designs that allow these components to be more clearly dissociated. Moreover, it would be useful to have direct cerebellar recordings as part of an exploration of the origin and propagation of timing signals.

Additionally, extending analyses to assess trial-by-trial correlations between neural features (e.g., LFP power) and behavioral precision may offer further insights into the functional relevance of the observed signals. Cross-regional coherence and computational modeling could also help delineate the distinct contributions of cerebellar-thalamic and basal ganglia pathways to sensory-guided *versus* internally generated timing [36].

Conclusion

This study provides direct electrophysiological evidence that behavioral timing in repetitive tasks is reflected in internal signals from basal ganglia and thalamic nuclei receiving cerebellar projections. Time-locked responses and frequency-specific oscillations were observed across both sensory-guided and internally generated phases of movement, highlighting the involvement of cerebellothalamic and basal ganglia pathways in temporal coordination. The relative timing in these areas may help to differentiate between regions responsible for cued *versus* autonomous behavior, and regions responsible for the generation of movement and those that respond to sensory effects of movement.

These findings enhance our understanding of the distributed neural substrates supporting motor timing in dystonia and suggest that targeting specific subcortical timing networks may improve the precision of DBS interventions.

Data availability statement

The data analyzed in this study is subject to the following licenses/restrictions: The datasets were collected as part of DBS procedure for clinical and research purposes. They are considered protected health information under HIPAA. De-identified datasets may be available on request. Requests to access these datasets should be directed to TS.

Ethics statement

The studies involving humans were approved by Children's Hospital of Orange County (CHOC). The studies were conducted in accordance with the local legislation and institutional requirements. Written informed consent for participation in this study was provided by the participants' legal guardians/next of kin. Written informed consent was obtained from the minor(s)' legal guardian/next of kin for the publication of any potentially identifiable images or data included in this article.

Author contributions

SS, SJ, MA, RI, and TS contributed to data acquisition, data analysis, data interpretation, and writing the manuscript. SS, RI, and TS conceived the study. All authors contributed to the article and approved the submitted version.

Funding

The authors declare that financial support was received for the research and/or publication of this article. This work was supported by funding from the Raynor Cerebellum Project and the National Institutes of Health (NIH R35NS116883).

Acknowledgements

We thank our volunteers and their parents for participating in this study. We thank Sumiko Abe for neuroimaging processing. We also thank Anna Brucker and Teresa Serna-Fonseca for their assistance with neurological examinations and data collection.

Conflict of interest

The authors declare that the research was conducted in the absence of any commercial or financial relationships that could be construed as a potential conflict of interest.

Generative AI statement

The authors declare that Generative AI was used in the creation of this manuscript. Portions of the manuscript text were refined for grammar and style using ChatGPT (GPT-5, OpenAI). The authors reviewed and edited all AI-generated material to ensure accuracy and take full responsibility for the content of the final manuscript.

Any alternative text (alt text) provided alongside figures in this article has been generated by Frontiers with the support of artificial intelligence and reasonable efforts have been made to ensure accuracy, including review by the authors wherever possible. If you identify any issues, please contact us.

References

1. Grube M, Cooper FE, Chinnery PF, Griffiths TD. Dissociation of duration-based and beat-based auditory timing in cerebellar degeneration. *Proc Natl Acad Sci* (2010) 107(25):11 597–11 601. doi:10.1073/pnas.0910473107

2. Baumann O, Borra RJ, Bower JM, Cullen KE, Habas C, Ivry RB, et al. Consensus paper: the role of the cerebellum in perceptual processes. *The Cerebellum* (2015) 14:197–220. doi:10.1007/s12311-014-0627-7

3. Ivry RB, Keele SW. Timing functions of the cerebellum. *J Cogn Neurosci* (1989) 1(2):136–52. doi:10.1162/jocn.1989.1.2.136

4. Bryant JL, Boughter JD, Gong S, LeDoux MS, Heck DH. Cerebellar cortical output encodes temporal aspects of rhythmic licking movements and is necessary for normal licking frequency. *Eur J Neurosci* (2010) 32(1):41–52. doi:10.1111/j.1460-9568.2010.07244.x

5. Ivry RB, Spencer RM. The neural representation of time. *Curr Opin Neurobiol* (2004) 14(2):225–32. doi:10.1016/j.conb.2004.03.013

6. Koziol LF, Budding D, Andreasen N, D'Arrigo S, Bulgheroni S, Imamizu H, et al. Consensus paper: the cerebellum's role in movement and cognition. *The Cerebellum* (2014) 13:151–77. doi:10.1007/s12311-013-0511-x

7. Fahn S. Concept and classification of dystonia. *Adv Neurol* (1988) 50:1–8.

8. Batla A, Sánchez M, Erro R, Ganos C, Stamelou M, Balint B, et al. The role of cerebellum in patients with late onset cervical/segmental dystonia? Evidence from the clinic. *Parkinsonism and Relat Disord* (2015) 21(11):1317–22. doi:10.1016/j.parkreldis.2015.09.013

9. Owen RL, Grewal SS, Thompson JM, Hassan A, Lee KH, Klassen BT. Effectiveness of thalamic ventralis oralis anterior and posterior nuclei deep brain stimulation for posttraumatic dystonia. *Mayo Clinic Proc Innov Qual and Outcomes* (2022) 6(2):137–42. doi:10.1016/j.mayocpiqo.2022.01.001

10. Zhuang P, Li Y, Hallett M. Neuronal activity in the basal ganglia and thalamus in patients with dystonia. *Clin Neurophysiol* (2004) 115(11):2542–57. doi:10.1016/j.clinph.2004.06.006

11. Obermann M, Yaldizli O, De Greiff A, Lachenmayer ML, Buhl AR, Tumczak F, et al. Morphometric changes of sensorimotor structures in focal dystonia. *Movement Disord* (2007) 22(8):1117–23. doi:10.1002/mds.21495

12. Malone A, Manto M, Hass C. *Dissecting the links between cerebellum and dystonia* (2014). p. 666–8.

13. LeDoux MS, Lorden JF, Ervin JM. Cerebellectomy eliminates the motor syndrome of the genetically dystonic rat. *Exp Neurol* (1993) 120(2):302–10. doi:10.1006/exnr.1993.1064

14. Adury RZ, Wilkes BJ, Girdhar P, Li Y, Vaillancourt DE. Altered functional brain connectivity in dyt1 knock-in mouse models. *Dystonia* (2025) 4:13874. doi:10.3389/dyst.2025.13874

15. Filip P, Lungu OV, Bareš M. Dystonia and the cerebellum: a new field of interest in movement disorders? *Clin Neurophysiol* (2013) 124(7):1269–76. doi:10.1016/j.clinph.2013.01.003

16. Milosevic L, Kalia SK, Hodaie M, Lozano AM, Popovic MR, Hutchison WD. Physiological mechanisms of thalamic ventral intermediate nucleus stimulation for tremor suppression. *Brain* (2018) 141(7):2142–55. doi:10.1093/brain/awy139

17. Asanuma C, Thach W, Jones E. Distribution of cerebellar terminations and their relation to other afferent terminations in the ventral lateral thalamic region of the monkey. *Brain Res Rev* (1983) 5(3):237–65. doi:10.1016/0165-0173(83)90015-2

18. Anderson ME, Turner RS. Activity of neurons in cerebellar-receiving and pallidal-receiving areas of the thalamus of the behaving monkey. *J Neurophysiol* (1991) 66(3):879–93. doi:10.1152/jn.1991.66.3.879

19. Kultas-Ilinsky K, Ilinsky I. Fine structure of the ventral lateral nucleus (vl) of the macaca mulatta thalamus: cell types and synaptology. *J Comp Neurol* (1991) 314(2):319–49. doi:10.1002/cne.903140209

20. Kuramoto E, Fujiyama F, Nakamura KC, Tanaka Y, Hioki H, Kaneko T. Complementary distribution of glutamatergic cerebellar and gabaergic basal ganglia afferents to the rat motor thalamic nuclei. *Eur J Neurosci* (2011) 33(1):95–109. doi:10.1111/j.1460-9568.2010.07481.x

21. Sakayori N, Kato S, Sugawara M, Setogawa S, Fukushima H, Ishikawa R, et al. Motor skills mediated through cerebellothalamic tracts projecting to the central lateral nucleus. *Mol Brain* (2019) 12:13–2. doi:10.1186/s13041-019-0431-x

22. Aumann T, Rawson J, Finkelstein D, Horne M. Projections from the lateral and interposed cerebellar nuclei to the thalamus of the rat: a light and electron microscopic study using single and double anterograde labelling. *J Comp Neurol* (1994) 349(2):165–81. doi:10.1002/cne.903490202

23. Teune T, Van Der Burg J, Van Der Moer J, Voogd J, Ruigrok TJ. Topography of cerebellar nuclear projections to the brain stem in the rat. *Prog Brain Res* (2000) 124:141–72. doi:10.1016/S0079-6123(00)24014-4

24. Liker M, Sanger T. Pediatric deep brain stimulation in secondary dystonia using stereotactic depth electrode targeting. *MOVEMENT DISORDERS* (2019) 34: S534–S535.

25. Liker MA, Sanger TD, MacLean JA, Nataraj J, Arguelles E, Krieger M, et al. Stereotactic awake basal ganglia electrophysiological recording and stimulation (sabers): a novel staged procedure for personalized targeting of deep brain stimulation in pediatric movement and neuropsychiatric disorders. *J Child Neurol* (2024) 39(1-2):33–44. doi:10.1177/08830738231224057

26. Ivry R. Cerebellar involvement in the explicit representation of temporal information a. *Ann New York Acad Sci* (1993) 682(1):214–30. doi:10.1111/j.1749-6632.1993.tb22970.x

27. Ivry RB, Spencer RM, Zelaznik HN, Diedrichsen J. The cerebellum and event timing. *Ann New York Acad Sci* (2002) 978(1):302–17. doi:10.1111/j.1749-6632.2002.tb07576.x

28. Ohmae S, Kunimatsu J, Tanaka M. Cerebellar roles in self-timing for sub-and supra-second intervals. *J Neurosci* (2017) 37(13):3511–22. doi:10.1523/JNEUROSCI.2221-16.2017

29. Hernandez-Martin E, Arguelles E, Liker M, Robison A, Sanger TD. Increased movement-related signals in both basal ganglia and cerebellar output pathways in two children with dystonia. *Front Neurol* (2022) 13:989340. doi:10.3389/fneur.2022.989340

30. Hernandez-Martin E, Kasiri M, Abe S, MacLean J, Olaya J, Liker M, et al. Globus pallidus internus activity increases during voluntary movement in children with dystonia. *Iscience* (2023) 26(7):107066. doi:10.1016/j.isci.2023.107066

31. Kasiri M, Javadzadeh S, Nataraj J, Seyyed Mousavi SA, Sanger T. Correlated activity in globus pallidus and thalamus during voluntary reaching movement in three children with primary dystonia. *Dystonia* (2023) 2:11117. doi:10.3389/dyst.2023.11117

32. Breska A, Ivry RB. Double dissociation of single-interval and rhythmic temporal prediction in cerebellar degeneration and parkinson's disease. *Proc Natl Acad Sci* (2018) 115(48):12 283–12 288. doi:10.1073/pnas.1810596115

33. Tanaka M, Kunimatsu J, Suzuki TW, Kameda M, Ohmae S, Uematsu A, et al. Roles of the cerebellum in motor preparation and prediction of timing. *Neuroscience* (2021) 462:220–34. doi:10.1016/j.neuroscience.2020.04.039

34. Théoret H, Haque J, Pascual-Leone A. Increased variability of paced finger tapping accuracy following repetitive magnetic stimulation of the cerebellum in humans. *Neurosci Lett* (2001) 306(1-2):29–32. doi:10.1016/s0304-3940(01)01860-2

35. Kasiri M, Asadi M, Nataraj J, Abe S, Sanger TD, Optimized dbs in pediatric dystonia restores balance in transmission of signals within pallidothalamic network by modulating neural oscillations in deep brain regions. *medRxiv*. (2025).

36. Asadi M, Javadzadeh S, Soroushmojdehi R, Mousavi SAS, Sanger T. Bace: Behavior-adaptive connectivity estimation for interpretable graphs of neural dynamics. *bioRxiv* (2025).